1   **Title:** Technical Note: Semi-automated effective width extraction from time-lapse RGB

2   imagery of a remote, braided Greenlandic river.

3   **Authors**: Colin J. Gleason[1], Laurence C. Smith[1], David C. Finnegan [2], Adam L. LeWinter [2],

4   Lincoln H Pitcher [1], Vena W. Chu[1]

5   **Author affiliation**:

6   1) Department of Geography, University of California-Los Angeles. 1255 Bunche Hall, 405

7   Hilgard Avenue, Los Angeles, California 90095-1524

8   2) U.S. Army Cold Regions Research & Engineering Laboratory, Hanover, NH 03755

9   **Corresponding Author**: C.J. Gleason, cjgleaso@ucla.edu

10   **Abstract:** River systems in remote environments are often challenging to monitor and

11   understand where traditional gauging apparatus are difficult to install or where safety

12   concerns prohibit field measurements. In such cases, remote sensing, especially terrestrial

13   time lapse imaging platforms, offer a means to better understand these fluvial systems. One

14   such environment is found at the proglacial Isortoq River in southwest Greenland, a river

15   with a constantly shifting floodplain and remote Arctic location that make gauging and *in*

16   *situ* measurements all but impossible. In order to derive relevant hydraulic parameters for

17   this river, two RGB cameras were installed in July of 2011, and these cameras collected

18   over 10,000 half hourly time-lapse images of the river by September of 2012. Existing

19   approaches for extracting hydraulic parameters from RGB imagery require manual or

20   supervised classification of images into water and non-water areas, a task that was

21   impractical for the volume of data in this study. As such, automated image filters were

22   developed that removed images with environmental obstacles (e.g. shadows, sun glint,

23   snow) from the processing stream. Further image filtering was accomplished via a novel

automated histogram similarity filtering process. This similarity filtering allowed

successful (mean accuracy 79.6%) supervised classification of filtered images from training

data collected from just 10% of those images. Effective width, a hydraulic parameter highly

correlated with discharge in braided rivers, was extracted from these classified images,

producing a hydrograph proxy for the Isortoq River between 2011 and 2012. This

hydrograph proxy shows agreement with historic flooding observed in other parts of

Greenland in July 2012 and offers promise that the imaging platform and processing

methodology presented here will be useful for future monitoring studies of remote rivers.

1. Introduction

Proglacial streams and rivers along land-terminating edges of the Greenland Ice

Sheet are among the world's most difficult fluvial systems to study in the field, owing to

their remoteness, harsh climate, and braided morphology. Discharge variations in large

proglacial rivers are of particular scientific interest, as these systems typically derive water

from the interior ablations surface Greenland Ice Sheet and are thus useful for inferring

runoff mass losses from the ice sheet (Rennermalm et al., 2013; Smith et al. 2014).

However, their high sediment loads, unstable banks, and dynamic braided channels present

challenges to traditional *in situ* river gauging techniques, and long term hydrographs for

these rivers are rare. While not unique to Greenland, these challenges are particularly

evident there, with more than 100 large (> 1 km width) large braided rivers exiting the ice

sheet with no observations of discharge whatsoever.

Where *in situ* methods are impractical, remotely sensed imagery offers an

increasingly viable option for obtaining scientifically useful estimates of river discharge in

1   remote or otherwise inaccessible areas (Smith et al., 1997, Ashmore and Sauks, 2006,

2   Durand et al., 2010, Gleason and Smith, 2014). Braided rivers in particular typically display

3   a power-law relationship between floodplain inundation area (which can be remotely

4   sensed) and discharge, which has been exploited using satellites, aerial imagery, and

5   terrestrial time-lapse photography (Smith 1995; 1996, Chandler *et al.*, 2002; Ashmore and

6   Sauks, 2006; Egozi and Ashmore 2008; Smith and Pavelsky, 2008; Bertoldi *et al.*, 2009;

7   Hundey and Ashmore, 2009; Bertoldi *et al.*, 2010; Bird *et al.*, 2010; Ashmore *et al.*, 2011;

8   Welber *et al.*, 2012; Williams *et al.*, 2013; Young *et al.*, 2015).

9   Regardless of the technology used, each remotely sensed image must first be

10   classified into areas of water and non-water, a task for which numerous methodologies

11   exist. In satellite remote sensing, NIR wavelength image bands can reliably detect open

12   water surfaces. However, satellite imagery often lacks the required spatial and temporal

13   resolution to adequately capture hydrologic phenomena, especially for smaller rivers. This

14   has led to the use of non-metric, true color (RGB) digital camera imagery to capture water

15   surfaces as an inexpensive and image-on-demand alternative to satellite and airborne

16   platforms, especially for braided rivers. To calculate hydraulic parameters (e.g. effective

17   width, braiding index, sinuosity, or bed slope elevation), these studies have commonly

18   classified water surfaces within images either manually or by supervised classification

19   (Egozi and Ashmore 2008; Bertoldi *et al.*, 2009; Hundey and Ashmore, 2009; Ashmore *et*

20   *al.*, 2011; Welber *et al.*, 2012). Another parameter estimation approach relies on water

21   surface delineation from automatically generated DEMs constructed from stereo-imagery

22   and other data sources (Chandler *et al.*, 2002; Ashmore and Sauks, 2006; Bird *et al.*, 2010;

23   Bertoldi *et al.*, 2010). Additionally, Young et al (2015) recently demonstrated the

1   effectiveness of calculating water stage change at a station from terrestrial

2   photogrammetry, which they combined with assumptions of channel geometry and

3   roughness to calculate river discharge via Manning's equation. This approach is highly

4   effective, but limited to situations where bathymetry is known or channel geometry may be

5   simply described. Finally, structure-from-motion, a technique that leverages multiple

6   vantage points of the same scene to reconstruct topography, has also been successfully

7   leveraged to calculate floodplain geometry and water surface elevation, but is again

8   impractical for long term monitoring with large data volumes (e.g. Fonstad *et al.,* 2013,

9   Javernick *et al.,* 2014).

10   While each of these studies successfully calculated hydrologic parameters from

11   remotely sensed images, their manual or time-intensive approaches are impractical for

12   large data volumes. This is especially an issue for long term hydrologic monitoring sorely

13   needed in many remote rivers, as using the image platform and processing developed by

14   Ashmore and Sauks(2006) and Welber *et al.* (2012), for instance, could easily generate tens

15   of thousands of images per year. Automated DEM generation methods would seem a ready

16   alternative, yet these require numerous fixed targets of known position to persist from

17   image to image, which are seldom found or are difficult to install on dynamic braided river

18   systems owing to their constantly shifting morphology. If such image platforms are to be

19   viable for long term monitoring studies, a systematic procedure for automatic image

20   quality selection and classification, preferably for RGB image data, is needed.

21   To that end, this paper proposes a semi-automated processing stream designed to

22   classify and extract hydraulic parameters of interest from large volumes of RGB image data

1   collected from a fixed terrestrial platform, and demonstrates its efficacy in a remote

2   Greenlandic river. Automated filters are developed that remove obstacles to image

3   classification based on easily calculated environmental variables, and an image similarity

4   filter is developed that allows supervised classification of many images from minimal

5   training data. Here, these filtering and classification techniques are employed to extract

6   effective width (W_e, inundation area divided by reach length), a hydraulic parameter that

7   has been shown to be highly correlated with discharge in braided rivers and has been

8   successfully extracted from remotely sensed data in proglacial environments (Smith *et*

9   *al.,*1996; Smith, 1997; Ashhmore and Sauks, 2006; Smith and Pavelsky, 2008; Ashmore *et*

10   *al.,* 2011). To evaluate the robustness of the extraction, we assess image classification

11   accuracy using manually generated ground truth data.

12   **2. Data**

13   This study was conducted on the proglacial Isortoq River in southwestern

14   Greenland. The Isortoq, one of the largest braided rivers draining the Greenland ice sheet,

15   issues from the Issunguata Sermia glacier terminus with discharge dominated by

16   meltwater outflow from the ablating ice surface (Smith et al., 2014). In July 2011, two

17   Nikon D200 model RGB cameras (focal lengths of 24 and 50mm) were installed 250m

18   above a reach of the Isortoq braid plain approximately 3.1 km downstream of the ice edge.

19   The camera system was identical to that developed by the Extreme Ice Survey project

20   (www.extremeicesurvey.org) for use in severe Arctic conditions. In addition to the

21   cameras, a modified battery pack and electronic controller were housed inside a

22   weatherproof case with an abrasion-resistant viewing window. The case was mounted on

1   a survey tripod and powered by a 12V gel battery recharged by solar panel. The cameras

2   were oriented so as to image sections of the braid plain of approximately 1.5km x 2.0km

3   and 2.0km x 2.3km, respectively (Figure 1), and captured one image every 30 minutes

4   when light conditions permitted.

5   Camera data collection commenced July 22nd, 2011, and over 10,000 images were

6   retrieved from the cameras by September 10th, 2012, covering most of two melt seasons.

7   The camera setup proved robust: the light sensor operated properly, the position of the

8   cameras remained unchanged, and the batteries powering the cameras were still functional

9   after the one year collection period for the wide focus camera. However, a presumed Arctic

10 fox chewed through the cables connecting the battery to the camera for the more narrowly

11 focused platform and halted data collection only two months after installation. Therefore,

12 all analyses presented in this paper refer to the wide focus camera, which remained

13 continuously operable throughout the study period July 22nd 2011 –September 10th 2012.

14 **3. Methods**

15   Classifying the RGB image data into water and non-water areas to extract W_e

16 presented several technical challenges for the 10,327 images that were collected by the

17 wide focus camera from July 2011 to September 2012. Existing approaches for hydraulic

18 parameter extraction from RGB data require either manual or supervised classification of

19 water within each image and are thus inappropriate for the large data volumes generated

20 in this study. Unsupervised classification techniques provide a straightforward alternative

21 for large time-lapse camera datasets, yet also present additional challenges as the images

22 collected here are extremely diverse and differing soil moisture in the braid plain gives the

1   appearance of multiple classes of output. Environmental factors such as time-varying solar

2   angles, blowing sand, dense fog, shadowing, snow and rain on the camera lens, and acute

3   sun-glint from water surface are especially prevalent in the Isortoq image data. These

4   factors were all addressed, and W_e accurately extracted, by the processing workflow

5   described below and presented in Figure 2.

6   *3.1 Environmental Filtering*

7   The first task for extracting W_e was to filter the large amount of image data into

8   those images that were most easily classified into water and non-water areas by

9   eliminating images containing the environmental obstacles described above. Once images

10   are classified, water area (and therefore W_e) may be calculated. Several filters were

11   developed to remove these poor quality images. First, images acquired during periods of

12   non-flow (before and after melt season activity) were culled. Next, images with shadowing

13   were culled by calculating the zenith and azimuth angles of the sun relative to the river

14   plain. Through visual inspection of the image time series, zenith angles less than 65 degrees

15   and azimuth angles between 245-290 and between 70-100 degrees were found to produce

16   shadows created by steep valley walls that prevented accurate classification (note valley

17   walls, Figures 1 and 2). Next, images that exhibited excessive sun glinting were removed.

18   Sun glint was defined as when an image exhibited either a ratio of the 95th brightness

19   percentile to the 5th brightness percentile greater than 1.8 or contained more than 1% of

20   pixels with brightness value greater than 215. This filter was necessary, as sun glint was

21   observed both on open water and saturated sand, making distinction between these very

22   different fluvial environments difficult (Figure 2). Successful application of these winter,

1 shadow, and sun glint filters culled 9,487 images from the image time series, leaving 840

2 images free of environmental obstacles that still captured every day of the two melt

3 seasons.

4 *3.2 Similarity Filtering*

5 Even with these stringent filters, unsupervised classification was still unable to

6 delineate water surfaces with satisfactory accuracy, and the number of images remaining

7 was still too large for supervised classification to be feasible. As such, a semi-supervised

8 classification approach was developed. To perform this classification, another image

9 filtering was needed to find images that were similar enough to one another to share

10 training data from a small sample of images in a supervised classification. The presence of

11 dense fog, blowing sand, or cloudiness changes the brightness values of the imagery, so

12 even images collected with identical solar geometry can be difficult to classify in an

13 unsupervised manner. A similarity filter was developed that selected images that not only

14 had similar solar geometry, but also had the same brightness and illumination and were all

15 free of environmental obstacles not covered by the first filtering.

16 This similarity filtering was accomplished by calculating and comparing the

17 histograms of each of the red, green, and blue bands for each image. Histograms of

18 brightness values that fell into 100 bins evenly spaced from 0 to 255 (reflectance values)

19 were calculated for each band of each image. Using the same bins for each image ensured

20 that cross comparison of images would not be affected by stretching of the image data.

21 Once these histograms were generated, the root mean square error (RMSE) between

22 histogram counts per bin was computed in a band-by-band pairwise permutation, giving a

23 per-image and per-band indication of the similarity of every image to each other image.

The pairwise permutation tests all possible image pairs for similarity. That is, for any given image, the histogram bin counts in each of its RGB bands is compared against bin counts of every other image and the RMSE (across all bins) of each comparison is recorded. Then, the process is repeated for every other image in the set, which yields $(n^2-n)/2$ RMSE values per image, where n is the number of images. These band-by-band RMSE values were then averaged to arrive at an overall measure of image similarity: here termed an image's similarity index. This metric was used to identify the 20% of the images that were most similar to each other, resulting in 168 images that were collected at similar sun angles without any environmental obstacles. Importantly, the similarity filter also produced images that contained four basic elements: dark (non-sun lit, turbid) water, bright (sun lit or non-turbid) water, dark (wet) sand, and bright (dry) sand (see Fig. 1c), thus producing images easily classified from lumped training data- a process described next.

3.3 Georectification and classification

Once the final filtering of images was complete, images were cropped to exclude the wide upstream floodplain and georectified into ground coordinates using a 4th degree polynomial transformation implemented in ENVI v4.8 (Figure 2). Eighty ground control points were manually extracted from a 2 m panchromatic World View 2 image acquired on September 23rd, 2011 (paired with a camera image collected 10 minutes later) and used to define the basis for the transformation. This warping polynomial was subsequently applied to all filtered images. After georectification, each image pixel had dimensions of 1m by 1m, an appropriate resolution for camera data collected at this scale. These georectified pixels allowed calculation of water surface area, and thus W_e, from the classified images.

1   To classify images into water and non-water areas for W_e extraction, training data

2   representing four classes (dark water, bright water, dark sand, and bright sand) were

3   manually collected from a random 10% sample (16 images) of the similarity filtered

4   images. The RGB statistics generated from these training polygons were applied to all

5   images passing the similarity filtering and used to train a maximum likelihood supervised

6   classification method performed in ENVI v4.8 for each image. This process requires that

7   each image has nearly identical RGB composition in order to be successful, which was

8   guaranteed by the similarity filtering.

9   **4. Results and discussion**

10   *4.1 Image Filtering*

11   The environmental and similarity filters developed in this study substantially

12   reduced the number of images available for W_e extraction from image collection to

13   classification. The automated environmental filtering removed 9,487 images with sun glint,

14   shadowing, or winter conditions, leaving 840 images for further operations. The similarity

15   filtering further reduced the image pool to 168 images that were ultimately passed to

16   classification and W_e extraction. This is obviously a large percentage of images removed,

17   but this stringent filtering left only very high quality images that were easily classified

18   using the semi-supervised approach. However, this high degree of culling still left images

19   with daily (or better) temporal resolution available for W_e extraction. If hourly or better

20   resolution images are needed, then the similarity filtering would need to be performed on

21   iterative batches of images, as there are other groups of images similar to one another that

22   are not similar to all images as a whole that are removed by the similarity filter. Each of

23   these groups could also be classified using their own lumped training data and output

1   classes determined by their composition. This would extend the temporal coverage of the

2   record, but since the similarity filter we propose yielded near daily coverage of the river we

3   felt this simplest case to be sufficient for the river in this study and did not identify further

4   groups of similar images.

5   Water turbidity could have effected this successful filtering. As sediment load and

6   river velocities change, water can appear darker or brighter depending on river turbidity,

7   thus affecting our choice of two water classes ('dark' and 'bright'). In the Isortoq, the

8   monitoring section is very close to the glacial terminus (~3.1km), and as such the sediment

9   load is fairly constant, the river well mixed, and sediment relatively unsorted, so 'bright' water

10   corresponds to sunlight water, rather than less turbid water. Given these conditions, the two

11   classes do cover nearly all the turbidity values observed in the Isortoq River after image

12   similarity filtering. In rivers with more variable turbidity or places where the bed is visible at

13   low flows, more water/non-water classes and different filters might be needed to adequately

14   cover the range of observed sediment loads.

15   *4.2 Accuracy assessment*

16   The semi-supervised classification described here proved an effective and unbiased

17   classification method. Figure 3 shows the overall accuracy, user's accuracy for water, and

18   user's accuracy for non-water as a function of W_e from a random sample of 56 images (33%

19   of filtered images). Accuracy was assessed using approximately 500 semi-random,

20   manually derived assessment points for each class (water and non-water) per image. Of

21   particular interest were both the overall accuracy (total number of correctly classified

22   assessment points divided by total number of assessment points, ~500), and the user's

23   accuracy for water and non-water (percentage of image pixels classified correctly as

1   assessed by the training data). These metrics provide an assessment of classification

2   performance from the standpoint of each classified image: the paradigm that speaks

3   directly to the fidelity of extracted W_e. Accuracy assessment indicates that overall accuracy

4   is acceptable (mean accuracy for the assessment sample is 79.6%), and neither overall

5   accuracy (r= -0.11) nor water user's accuracy (r= 0.35) show strong correlation with W_e.

6   This lack of correlation indicates that the classification of water is not affected by the extent

7   of water inundation in the scene. There is a strong correlation (r=-0.79) between the user's

8   accuracy of non-water pixels and W_e, but this negative correlation is a reflection of the

9   difficulty of classifying the small number of non-water pixels remaining in scenes where

10   the braid plain was nearly completely flooded. The reason for this successful classification

11   was the similarity of filtered images, which was guaranteed by the similarity index

12   procedure described above. After classification, W_e was calculated as the area of classified

13   water within a 1,000m reach located where the image data provided complete bank to

14   bank coverage, indicated by the magenta polygons (dashed) in Figure 2.

15   *4.3 Extracted* W_e *hydrograph*

16   The W_e hydrograph shown in Figure 4 is a proxy for discharge variations in the

17   Isortoq River from 2011-2012. Gaps in the date record indicate that there were no images

18   that passed filtering on those dates, even though images were acquired half hourly. This is

19   a result of prolonged rain events, heavy fog, or strong winds that caused images to be non-

20   similar during these days. Despite these gaps, the data record still provides near daily

21   coverage, indicating that filtering did not substantially affect the temporal distribution of

22   the output data. Of note is the large peak in W_e seen in July of 2012, coinciding with historic

23   melting of the Greenland ice sheet (Hall et al., 2013; Tedesco et al., 2013) and destruction of

the Watson River bridge in the town of Kangerlussuaq (Smith et al., 2014), located

approximately 15km south of the Isortoq River.

Figure 4 also reveals that the relative magnitude of W_e during this melt event was an

order of magnitude greater than W_e in low flow stages. This shows that the Isortoq River

behaves like other braided rivers with non-cohesive bed material, as its width adjusts

rapidly to changing discharge. In addition, the peak W_e observed here corresponds to

almost complete floodplain occupation by the river, highlighting the difficulty of installing

traditional gauging equipment at this site.

5. Conclusions

This paper has demonstrated the efficacy of a fixed position RGB time-lapse camera

platform for hydraulic parameter extraction for a large proglacial braided river in a remote

area of Greenland. The operational camera delivered over 10,000 half hourly images in just

over one year of collection, and demonstrated remarkable climactic resilience in the

Greenlandic winter. The other camera, however, was lost to a wildlife attack, pointing to

the need for stronger housing for all camera components. Such a platform is useful for

extraction of multiple hydraulic parameters, including effective width (W_e), a proxy for

discharge variations. To fully realize this monitoring potential, the W_e variations extracted

for each image could be calibrated with a rating curve built from intermittent field data.

The above accuracy assessments indicate that the semi-supervised classification

method produced accurate and unbiased results. An accurately delineated water surface is

necessary to preserve the fidelity of extracted hydraulic parameters. The processing

techniques described in this paper fall short of completely automated processing, yet this

paper does present an analysis protocol that achieves a consistent standard of classification from images that are automatically selected for ease of classification. Furthermore, the similarity filtering presented herein allows for supervised classification of numerous images from minimal training data, enabling long term hydrologic records to be maintained without onerous manual classification of imagery or photogrammetrically challenging DEM extraction.

6. Works cited

Ashmore, P., and Sauks, E.: Prediction of discharge from water surface width in a braided river with implications for at-a-station hydraulic geometry, Water Resources Research, 42, 10.1029/2005wr003993, 2006.

Ashmore, P., Bertoldi, W., and Gardner, J. T.: Active width of gravel-bed braided rivers, Earth Surface Processes and Landforms, 36, 10.1002/esp.2182, 2011.

Bertoldi, W., Zanoni, L., and Tubino, M.: Planform dynamics of braided streams, Earth Surface Processes and Landforms, 34, 547-557, 10.1002/esp.1755, 2009.

Bertoldi, W., Zanoni, L., and Tubino, M.: Assessment of morphological changes induced by flow and flood pulses in a gravel bed braided river: The Tagliamento River (Italy), Geomorphology, 114, 348-360, 10.1016/j.geomorph.2009.07.017, 2010.

Bird, S., Hogan, D., and Schwab, J.: Photogrammetric monitoring of small streams under a riparian forest canopy, Earth Surface Processes and Landforms, 35, 952-970, 2010.

Chandler, J., Ashmore, P., Paola, C., Gooch, M., and Varkaris, F.: Monitoring river-channel change using terrestrial oblique digital imagery and automated digital photogrammetry, Annals of the Association of American Geographers, 92, 631-644, 10.1111/1467-8306.00308, 2002.

Durand, M., Rodriguez, E., Alsdorf, D.E., and Trigg, M. Estimating river depth from remote sensing swath interferometry measurements of river height, slope, and width. IEEE Journal of Selected Topics in Applied Earth Observations and Remote Sensing, 3, 20-31, 10.1109/jstars.2009.2033453, 2010.

Egozi, R., and Ashmore, P.: Defining and measuring braiding intensity, Earth Surface Processes and Landforms, 33, 2121-2138, 10.1002/esp.1658, 2008.

Fonstad, M.A., Dietrich, J.T., Courville, B.C., Jensen, J.L., and Carbonneau, P.: Topographic structure from motion: a new development in photogrammetric measurement. Earth Surface Processes and Landforms, 38, 421-430. 10.1002/esp.3366. 2013.

Gilvear, D. J., Davids, C., and Tyler, A. N.: The use of remotely sensed data to detect channel hydromorphology; River Tummel, Scotland, River Research and Applications, 20, 795-811, 10.1002/rra.792, 2004.

Gleason, C.J., and Smith, L.C. Toward global mapping of river discharge using satellite images and at-many-stations hydraulic geometry. Proceedings of the National Academy of Sciences, 11, 4788-4791, 10.1073/pnas.1317606111, 2014.

Hall, D.K., Comiso, J.C., DiGirolamo, N.E., Shuman, C.A., Box, J.E., and Koenig, L.S. Variability in the surface temperature and melt extent of the Greenland ice sheet. Geophysical Research Letters, 40, 2114-2120, 10.1002/grl.50240, 2013.

Hundey, E. J., and Ashmore, P. E.: Length scale of braided river morphology, Water Resources Research, 45, 10.1029/2008wr007521, 2009.

Javernick, L., J. Brasington, and Caruso, B.:, Modelling the topography of shallow braided rivers using Structure-from-Motion photogrammetry, Geomorphology, 213, 166-182, 10.1016/j.geomorph.2014.01.006. 2014.

Rennermalm, A.K., Smith, L.C., Chu, V.W., Box, J.E., Forster, R.R., Van den Broeke, M.R., Van As, D., and Moustafa, S.E. Evidence of meltwater retention within the Greenland ice sheet. The Cryosphere, 7, 1433–1445, 10.5194/tc-7-1433-2013, 2013.

Smith, L. C., Isacks, B. L., Bloom, A. L., and Murray, A. B.: Estimation of discharge from three braided rivers using synthetic aperture radar satellite imagery: Potential application to ungaged basins, Water Resources Research, 32, 2021-2034, 10.1029/96wr00752, 1996.

1   Smith, L. C.: Satellite remote sensing of river inundation area, stage, and discharge: A

2   review, Hydrological Processes, 11, 1427-1439, 10.1002/(sici)1099-

3   1085(199708)11:10<1427::aid-hyp473>3.3.co;2-j, 1997.

4   Smith, L. C., and Pavelsky, T. M.: Estimation of river discharge, propagation speed, and

5   hydraulic geometry from space: Lena River, Siberia, Water Resources Research, 44,

6   10.1029/2007wr006133, 2008.

7   Smith, L.C., Chu, V.W., Yang, K., Gleason, C.J., Pitcher, Lincoln H, Rennermalm, A.K.,

8   Leglieter, C.J., Behar, A.E., Overstreet, B.T., Moustafa, S.E., Tedesco, M., Forster, R.R.,

9   LeWinter, A.L., Finnegan, D.C., Sheng, Y., and Balog, J. Efficient meltwater drainage through

10   supraglacial streams and rivers on the southwest Greenland ice sheet. Proceedings of the

11   National Academy of Sciences, in press, 2014.

12   Tedesco, M., Fettweis, X., Mote, T., Wahr, J., Alexander, P., Box, J.E., and Wouters, B.

13   Evidence and analysis of 2012 Greenland records from spaceborne observations, a

14   regional climate model, and reanalysis data. The Cryosphere, 7, 615-630, 10.5194/tc-7-

15   615-2013, 2013.

16   Welber, M., Bertoldi, W., and Tubino, M.: The response of braided planform configuration

17   to flow variations, bed reworking and vegetation: the case of the Tagliamento River, Italy,

18   Earth Surface Processes and Landforms, 37, 572-582, 10.1002/esp.3196, 2012.

19   Williams, R. D., J. Brasington, M. Hicks, R. Measures, C. D. Rennie, and Vericat, D.: Hydraulic

20   validation of two-dimensional simulations of braided river flow with spatially continuous

21   adcp data, Water Resources Research, 49, 5183-5205, 10.1002/wrcr.20391, 2013.

1   Young, D. S., J. K. Hart, and Martinez, K.: Image analysis techniques to estimate river

2   discharge using time-lapse cameras in remote locations, Computers &Geosciences, 76, 1-

3   10,/10.1016/j.cageo.2014.11.008. 2015

4

5   **Figure 1.** Figure 1 shows example images taken on July 17, 2012 of the Isortoq River by the

6   two camera systems as well as the cameras themselves (foreground and background, panel

7   a). The Issunguata Sermia Glacier is seen in the background, and nearly all water in this

8   river is derived from its melting terminus. Only the wide focus camera (c) has a continuous

9   data record from 2011-2012, as a presumed Arctic fox severed the wiring on the narrow

10   focus camera. The yellow polygon in the wide focus image shows the target reach for W_e

11   extraction, covering an area of approximately 1,000 by 2,000m.

12   **Figure 2.** The processing steps required to extract W_e from raw images are shown here.

13   Every step until the final classification is completely automated, allowing for a vast

14   reduction in processing time. Winter images were selected by a manual inspection of first

15   and last observed open water flow. Shadowing was defined as when solar zenith angles

16   were less than 65 degrees or solar azimuth between 245-290 or70-100 degrees, and sun

17   glint was defined as a ratio of pixel brightness and as a total pixel value threshold. As Figure

18   4 shows, these filters did not significantly affect the temporality of the data and almost

19   every day during the two melt season study duration is represented.

20   **Figure 3.** Accuracy assessment as a function of W_e from a 33% sample of post filtered

21   images is presented here, with overall accuracy (a), water user's accuracy (b), and non-

22   water user's accuracy (c) all showing acceptable performance. Overall accuracy and water

1   user's accuracy are not strongly correlated with W_e, suggesting that the amount of water in

2   the scene does not strongly influence the calculation of water area. Non-water accuracy,

3   however, is strongly affected by the amount of water in the scene as the Isortoq River

4   occupies nearly the entire valley at high flow, making classification of a few scattered non-

5   water pixels challenging.

6   **Figure 4.** Successful image classification allowed for extraction of W_e across two melt

7   seasons from the wide angle camera and gives a proxy for discharge in the braided Isortoq

8   River. 22 statistical outliers, representing poorly classified images, were removed before

9   generating this figure. These W_e time series clearly show historic flooding in Greenland in

10   July of 2012, as well as the abrupt start of the 2012 melt season, and suggest that the

11   camera platform and semi-automated classification techniques advanced here are

12   sufficient for monitoring of this remote river.

13
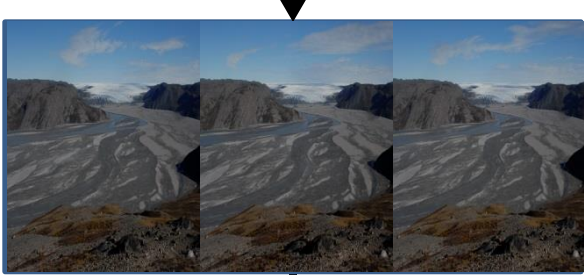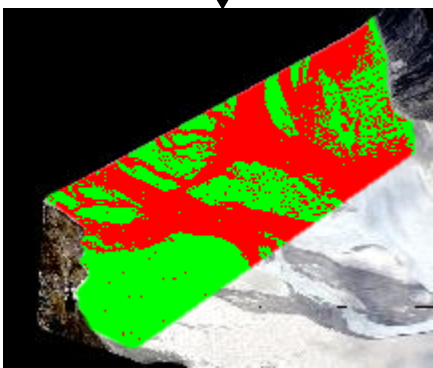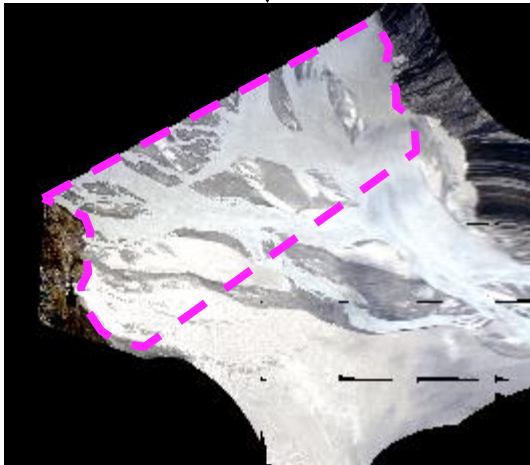
Remove winter images

Remove shadows

Remove sun glint

Perform similarity filtering
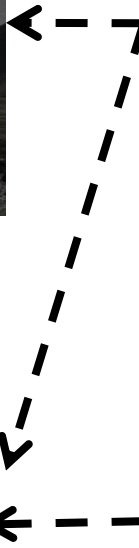
post filtering

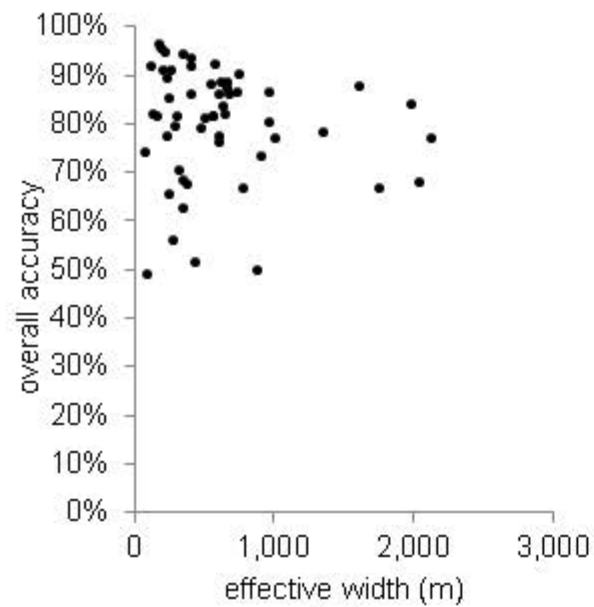Warp images to ground coordinates
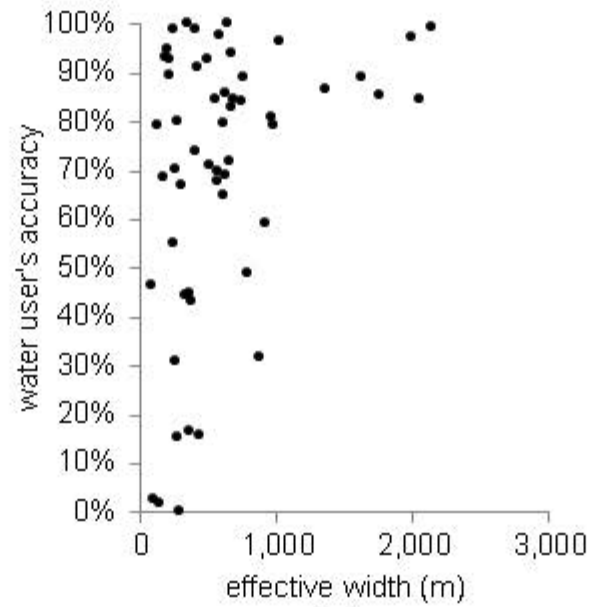
Collect training data from 10% of images
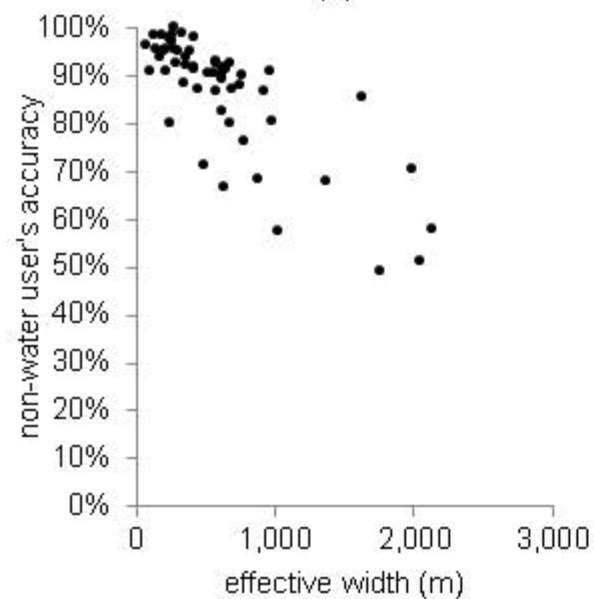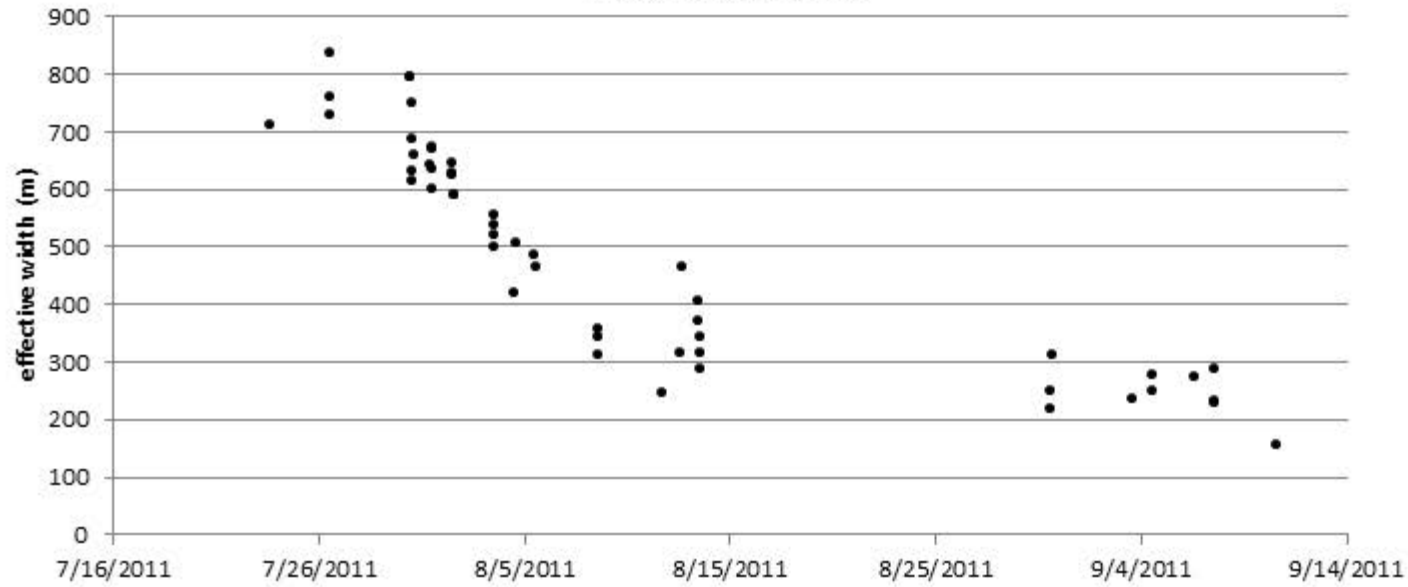
Classify all images from 10% training data

(a)

(b)

(c)

Melt Season 1

Melt Season 2